Biomaterials 52 (2015) 452–462

Contents lists available at ScienceDirect

Biomaterials

journal homepage: www.elsevier.com/locate/biomaterials

Engineered cartilaginous tubes for tracheal tissue replacement via self-assembly and fusion of human mesenchymal stem cell constructs

Anna D. Dikina [a], Hannah A. Strobel [b], Bradley P. Lai [a], Marsha W. Rolle [b], Eben Alsberg [a, c, *]

[a] Department of Biomedical Engineering, Case Western Reserve University, 10900 Euclid Ave, Cleveland, OH 44106, USA
[b] Department of Biomedical Engineering, Worcester Polytechnic Institute, 100 Institute Rd., Worcester, MA 01609, USA
[c] Department of Orthopaedic Surgery, Case Western Reserve University, 10900 Euclid Ave, Cleveland, OH 44106, USA

ARTICLE INFO

Article history:
Received 24 November 2014
Accepted 25 January 2015
Available online

Keywords:
Cartilage tissue engineering
Scaffold-free constructs
Custom culture wells
Tissue rings
Microspheres

ABSTRACT

There is a critical need to engineer a neotrachea because currently there are no long-term treatments for tracheal stenoses affecting large portions of the airway. In this work, a modular tracheal tissue replacement strategy was developed. High-cell density, scaffold-free human mesenchymal stem cell-derived cartilaginous rings and tubes were successfully generated through employment of custom designed culture wells and a ring-to-tube assembly system. Furthermore, incorporation of transforming growth factor-β1-delivering gelatin microspheres into the engineered tissues enhanced chondrogenesis with regard to tissue size and matrix production and distribution in the ring- and tube-shaped constructs, as well as luminal rigidity of the tubes. Importantly, all engineered tissues had similar or improved biomechanical properties compared to rat tracheas, which suggests they could be transplanted into a small animal model for airway defects. The modular, bottom up approach used to grow stem cell-based cartilaginous tubes in this report is a promising platform to engineer complex organs (e.g., trachea), with control over tissue size and geometry, and has the potential to be used to generate autologous tissue implants for human clinical applications.

1. Introduction

Narrowing or collapse of the trachea is a life threatening condition because stenosis or malacia can prohibit sufficient air transport to the lungs. The most common cause of adult tracheal stenosis is iatrogenic trauma due to prolonged intubation or tracheostomy, but other causes include perichondritis, chondritis, tumor, burns and external trauma [1–3]. Typically, if the affected portion is less than half the entire length of the trachea in adults or one third in children, the diseased region can be resected and the healthy ends anastomosed during tracheal reconstruction surgery [2,4]. While short, resectable stenoses are far more common, there are limited treatments available for lengthy tracheal occlusions. Short-term solutions for patients with long segment stenosis include stents, T-tubes, laser surgery and airway dilation. However, a major drawback to these is the need for repetitive treatment: periodic stent and tube replacement due to granuloma formation or additional laser surgery and dilation due to scarring and restenosis [5,6].

As a result, biomaterial and tissue engineering approaches have been pursued to develop tracheal substitutes. A functional tracheal replacement must first and foremost maintain airway patency during normal breathing. Normally, healthy tracheal cartilage supports the open windpipe. Acellular tracheal prostheses are constructed of rigid materials and tissue engineered cell-laden technologies are typically cartilaginous structures that are designed to mimic the trachea. A variety of tracheal replacement strategies have been explored, including cell-free artificial prostheses [7–9], autografts [10,11], native or decellularized allografts which are often seeded with the recipient's cells [12–18], and autologous de novo tissue engineered constructs [19–22]. Despite the broad range of approaches, each has shortcomings. Acellular tracheal prostheses often result in tissue granulation, implant migration, progressive scar tissue formation and restenosis [4,11]. Autografts and allografts have limited availability, poor mechanical

* Corresponding author. Department of Biomedical Engineering, Case Western Reserve University, 10900 Euclid Ave, Cleveland, OH 44106, USA. Tel.: +1 216 368 6425; fax: +1 216 368 1509.
E-mail address: eben.alsberg@case.edu (E. Alsberg).

http://dx.doi.org/10.1016/j.biomaterials.2015.01.073
0142-9612/

properties, and undergo remodeling upon implantation, often leading to collapse, scarring and airway occlusion [4,11]. Allogeneic donor tissue also carries a risk of disease transmission and immunogenicity; recipients of native tissues must be immunosuppressed and extra care must be taken to remove antigens from decellularized tissues. Tissue engineered constructs comprised of autologous cells in scaffolds circumvent immune response issues, but the structural, physical and biochemical properties of the scaffold must be carefully designed to guide cell behavior and neotissue formation. It is also challenging to tune the scaffold degradation rate to match that of cell proliferation and new extracellular matrix (ECM) production, and biomaterial degradation byproducts may hinder tissue healing [4,23].

A 3D scaffold-free approach for autologous tracheal engineering allows for increased cell–cell interactions which help recapitulate de novo tissue formation in a biomimetic environment that lacks an exogenous scaffold [24]. Increased intercellular communication and signaling in a scaffold-free system may enhance ECM synthesis and remodeling as well as provide a greater potential for tissue integration upon implantation [24]. While scaffold-free culture systems have recently been pursued in efforts to engineer cartilage for tracheal replacement applications [21,25,26], these reports used fully differentiated chondrocytes as a cell source. Engineering a construct with mature cells necessitates taking a biopsy from existing tissues, which may cause morbidity and pain at the donor site, and potential loss or diminished function of the donor organ. These concerns are particularly relevant in the case of cartilage where collection of a biopsy may require an invasive surgery and tissue regeneration is limited. In addition to complications at the harvest site, cartilage tissues have low cellularity and isolated chondrocytes are prone to lose their function during cell expansion [27]. Due to these challenges, utilization of fully differentiated chondrocytes for an autologous engineered cartilage therapy may be difficult to implement clinically. In contrast, mesenchymal stem cells (MSCs) are an attractive, clinically relevant cell source for neocartilage formation. MSCs can be harvested from the bone marrow of the patient with a minimally invasive procedure and easily expanded *in vitro* to achieve necessary cell numbers. This stem cell pool can then be differentiated into a variety of connective tissue cell phenotypes, including chondrocytes for the formation of cartilage tissue [28,29].

Bone marrow derived MSCs undergo chondrogenesis when cultured in high-cell density conformations with supplementation of transforming growth factor beta (TGF-β) [30]. High-density MSC-based methods to drive cartilage formation include micromass [31], aggregate or pellet [30], or sheet cultures [32]. Recently, a few groups have explored other culture geometries for cartilage tissue engineering, like seeding chondrocytes in oval molds for meniscal engineering [33], wrapping stacked chondrocyte-derived cartilage sheets around a tube for *in vivo* fusing [21] and fusing MSC-derived aggregates for condylar resurfacing [34]. A viable tracheal tissue replacement therapy using a scaffold-free strategy necessitates ring-shaped and tubular constructs of specific sizes. Compared to fusion of tissue sheets and spherical aggregates, the use of ring-shaped building blocks for forming a tube for tracheal tissue engineering avoids the need for circumferential fusing and may provide improved mechanical properties in resisting collapse of the lumen. To control tissue geometry, we have previously reported the use of annular molded culture wells for the creation of toroid vascular tissues and a tissue assembly system for the fusion of rings into tissue tubes [35].

Standard tissue culture, which relies on exogenously supplied growth factor, has the challenge of guiding scaffold-free stem cells to generate sizeable tissues with homogenous matrix distribution due to spatial non-uniformity of growth factor availability. Cells on the interior of the construct are exposed to less growth factor because a disproportionate amount is consumed by cells on the periphery of the tissue, and the remainder of the growth factor must diffuse through the thickness of the construct to reach cells deeper within the construct. To address the problem of diffusion limitations and to improve the spatial uniformity and temporal presentation of growth factors within these constructs, our lab has engineered a system for delivery of growth factor from within high-cell density stem cell cultures using microspheres [36]. This approach has resulted in engineered neocartilage with similar [37] or enhanced matrix production and uniformity, mechanical properties and tissue thickness compared to cell-only constructs where growth factor was delivered in the media [38,39] when growth factors were delivered with proteolytically-degradable gelatin microspheres.

In this study a tracheal tissue replacement strategy is demonstrated using a bottom-up approach for production of human MSC (hMSC)-derived cartilaginous rings and tubes through employment of custom designed culture wells and an assembly system. This technology is then used to test the hypothesis that incorporation of chondrogenic growth factor-delivering microspheres into the ring and tube-shaped high-cell density constructs enhances chondrogenesis with regard to mechanical properties and matrix production and distribution to provide functional tracheal patency in future clinical applications.

2. Methods

2.1. Experimental design

The work described here investigated the formation of engineered cartilaginous rings and tubes in custom designed molds. hMSCs alone ("hMSC") or with bioactive factor-releasing biopolymer microspheres ("hMSC + MS") were seeded in annular agarose wells to form scaffold-free, self-assembled three-dimensional tissue rings. Subsequently, tissue rings were stacked in 3-ring or 6-ring conformations to fuse into tissue tubes. Chondrogenesis was induced in rings and tubes during 22 days of *in vitro* culture after which constructs were harvested for analysis. A schematic of the ring and tube formation procedure is shown in Fig. 1.

2.2. hMSC isolation and culture

hMSCs were isolated from bone marrow aspirates obtained from the Case Comprehensive Cancer Center Hematopoietic Biorepository and Cellular Therapy Core under University Hospitals of Cleveland Institutional Review Board approval, as

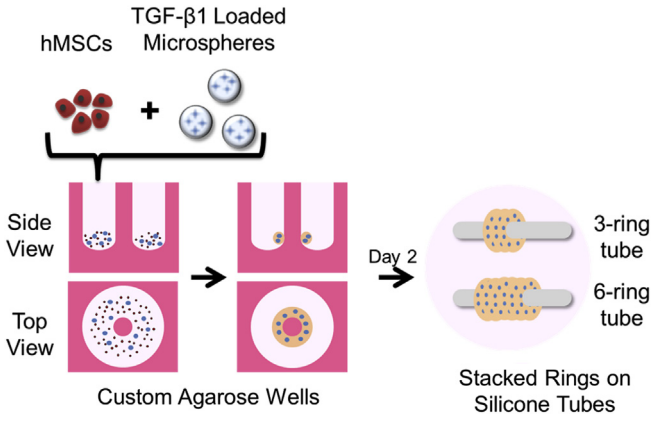

Fig. 1. Schematic of tissue ring and tube assembly processes. A suspension of MSCs with growth factor loaded microspheres ("hMSC + MS") was seeded in custom agarose (pink) wells and cultured in basal pellet media. Cell only tissues ("hMSC"), which did not contain microspheres, were seeded and cultured in basal pellet media supplemented with TGF-β1. On day 2 of culture, rings (tan) were removed from the culture wells using tweezers and were stacked on silicone tubes (gray) to form 3- and 6-ring tubes. (For interpretation of the references to color in this figure legend, the reader is referred to the web version of this article.)

previously described [40]. Briefly, bone marrow aspirates were washed with expansion media (Dulbecco's Modified Eagle's Medium—low glucose (DMEM-LG; Sigma—Aldrich, St. Louis, MO) containing 10% pre-screened bovine serum (Gibco Qualified FBS; Life Technologies, Carlsbad, CA)) [41]. Mononuclear cells were separated using a Percoll gradient (Sigma—Aldrich), plated in expansion media and cultured in a 37 °C humidified incubator with 5% CO_2. Non-adherent cells were washed away during the first media change. Adherent cells received fresh expansion media supplemented with 10 ng/ml fibroblast growth factor-2 (FGF-2, R&D Systems, Minneapolis, MN) every 2—3 days. The hMSCs were subcultured at ~90% confluence, and passage 3 cells were used in this study.

2.3. Microsphere synthesis and characterization

Gelatin microspheres (11.1 w/v% Type A; Sigma—Aldrich) were synthesized in a water-in-oil emulsion, as previously described, with slight modifications [39]. Microspheres were crosslinked with 1 w/v% genipin for 3 h (Wako Chemicals USA Inc., Richmond, VA), washed with deionized H_2O, lyophilized and rehydrated with Dulbecco's Phosphate Buffered Saline (PBS; HyClone Laboratories, Logan, UT) containing 400 ng TGF-β1 (PeproTech, Rocky Hill, NJ) per mg microspheres [39]. Light microscopy images of hydrated, crosslinked microspheres (N = 268) were acquired on a TMS microscope (Nikon, Tokyo, Japan) with a Coolpix 995 camera (Nikon) to determine microsphere diameters, which were measured using NIH Image J analysis software. The degree of microsphere crosslinking was quantified via a ninhydrin assay, based on a previously described protocol [39]. Here, the ninhydrin solution was added to dry microspheres and incubated for 2.5 min.

2.4. Cell culture well preparation

Agarose molds for cell culture were prepared as previously described [35]. Briefly, a polycarbonate sheet (Small Parts Inc., Miramar, FL) was machined to contain annular wells with concentric 2 mm diameter posts surrounded by a 3.75 mm wide trough. A polydimethylsiloxane (PDMS; Sylgard 184, Dow Corning, Midland, MI) negative mold of the polycarbonate template was cured and steam autoclaved for sterilization. Two percent w/v agarose (Denville Scientific Inc., Metuchen, NJ) in DMEM-LG was autoclaved and used to fill the PDMS mold. After cooling, the ring-shaped culture wells were removed from the PDMS mold, moved into 6-well plates (BD, Franklin Lakes, NJ) and incubated overnight in basal pellet medium (BPM) comprised of Dulbecco's Modified Eagle's Medium—high glucose (DMEM-HG; Sigma—Aldrich), 1% ITS + Premix (Corning Inc, Corning, NY), 10^{-7} M dexamethasone (MP Biomedicals, Solon, OH), 1 mM sodium pyruvate (HyClone Laboratories), 100 μM non-essential amino acids (Lonza Group, Basel, Switzerland), 37.5 μg/ml ascorbic acid-2-phosphate (Wako Chemicals USA Inc.) and 100 U/ml penicillin-streptomycin (Corning Inc.).

2.5. Assembly of microsphere-containing tissue rings and tubes

Trypsinized hMSCs (400,000 cells) with or without 0.3 mg TGF-β1 laden microspheres in 50 μL media were seeded in a circular fashion in each custom designed annular well. Microsphere-containing tissues ("hMSC + MS") were seeded and cultured in BPM. hMSC-only groups ("hMSC") did not contain microspheres and were seeded and cultured in BPM supplemented with 10 ng/ml TGF-β1. After 24 h, 3 ml of experimental condition-specific media were added to the agarose wells. On day 2, some of the self-assembled rings were transferred from the annular wells onto 2 mm silicone tubes (Specialty Manufacturing Inc., Saginaw, MI) to form 3- and 6-ring tissue tubes. Silicone tubes were sandwiched between custom engineered polycarbonate holders and the developing tissue tubes were cultured horizontally in 60 mm petri dishes (BD) containing 4.8—6 million cells and 9 ml of condition-specific media. A schematic of the tissue ring and tube assembly processes is shown in Fig. 1. A Galaxy S4 phone camera (Samsung, Seoul, Korea) was used to capture images of the custom culture set-up right after tissue tube assembly. Tissue rings and tubes with and without microspheres were grown in a humidified cell culture incubator at 37 °C and 5% CO_2 for 22 days with media changes every 2 and 3 days, respectively.

2.6. Gross morphological assessment

On day 22 of total culture, rings (22 days of culture as rings) and tubes (2 days of culture as rings followed by 20 days of culture as tubes) were harvested and photographs of all tissues were taken with a Galaxy S4 phone camera. Healthy, native rat tracheas (male NIH Nude rats 14—15 weeks old (N = 4); Taconic, Hudson, NY), freshly harvested from rats sacrificed for another study in accordance to a protocol approved by the Institutional Animal Care and Usage Committee at Case Western Reserve University, were used for comparison.

2.7. Biochemical analysis

Tissue rings (N = 4) and 3-ring tubes (N = 3) were digested in papain solution (Sigma—Aldrich) [42] at 65 °C. GAG and DNA contents were measured using dimethylmethylene blue (DMMB; Sigma—Aldrich) [43] and PicoGreen (Invitrogen, Carlsbad, CA) assays, respectively [44].

2.8. Histology and immunohistochemistry

Tissue rings and 3-ring tubes (N ≥ 2) were fixed in 10% neutral buffered formalin overnight, embedded in paraffin and sectioned at 5 microns. Rings were sectioned in either axial or vertical planes. Tubes were sectioned first in the axial plane and then re-embedded in paraffin and sectioned in the vertical plane. Mounted tissue sections were deparaffinized and rehydrated. Safranin O (Acros Organics) was used to stain for sulfated GAG content with a Fast Green counterstain (Fisher Chemical). For immunohistochemical staining, the presence of type II collagen was detected using anti-collagen type II primary antibody (abcam ab34712, Cambridge, UK) with a Fast Green counterstain. A section of the human knee articular cartilage and underlying subchondral bone served as a positive and negative control, respectively. Samples stained with isotype-matched IgG instead of primary antibody also served as negative controls. Histostain-Plus Bulk kit (Invitrogen) with aminoethyl carbazole (AEC; Invitrogen) was used to visualize the primary antibody. Images of stained tissues were acquired using an Olympus BX61VS microscope (Olympus, Center Valley, PA) with a Pike F-505 camera (Allied Vision Technologies, Stadtroda, Germany).

2.9. Tissue dimension measurements and biomechanical analysis

2.9.1. Rings

Day 21 tissue engineered rings and rat tracheal sections were sent in chondrogenic media from Case Western Reserve University to Worcester Polytechnic Institute (transit time was 3 nights and 1 night, respectively). Rings were then allowed to equilibrate for approximately 2 h in a 37 °C incubator prior to mechanical testing. Tissue ring wall thickness was measured in PBS using a machine vision system (DVT Model 630; DVT Corporation, Atlanta, GA). Measurements were taken in four locations around each ring using edge detection software (Framework 2.4.6; DVT), and the average thickness was used to calculate the average cross-sectional area. Each rat trachea was also measured in four locations, but using calipers due to its more uneven shape. Tissue engineered rings with and without microspheres and rat trachea sections were tested in uniaxial tension (ElectroPuls E1000 with a 50 N load cell; Instron, Norwood, MA) using a modified version of a system described previously [35]. Briefly, small stainless steel pins were bent into an "L" shape and served as grips for individual rings (Fig. 8A inset). After applying a 5 mN tare load, engineered rings were pulled in tension to failure at a rate of 10 mm/min. PBS was dripped on tissues during testing to prevent drying. From this test, the maximum load the rings could withstand was calculated. The ultimate tensile stress (UTS) was calculated by dividing the failure load by the cross-sectional area. Each engineered ring was approximated as a torus and each native trachea section was approximated as a hollow cylinder.

2.9.2. Tubes

Tissue engineered 6-ring tubes and 8 mm sections of rat trachea were equilibrated in PBS with 0.1% protease inhibitor (Sigma—Aldrich), and their outer diameters were measured by applying a pre-load of 3 mN with an R Series Controller mechanical testing device (Test Resources Inc., Shakopee, MN). Individual tubes and tracheas were tested in luminal collapse as previously described with modifications [9]. Each tube and trachea was compressed by 2 mm (luminal diameter) at a rate of 0.5 mm/min. The load was held for 6 min and then was removed at a rate of 60 mm/min. The load to collapse the lumen by 80% (1.6 mm) was used for comparison between the engineered tubes and rat tracheas. This was done to ensure that only the load required to collapse the lumen without compressing the walls of the tube was analyzed. Tube outside diameter was measured again after a 5 min no-load period. Percent luminal recoil was calculated as the ratio of the final outer diameter/initial outer diameter *100. Video recordings (Galaxy S4 phone camera) were taken of a representative hMSC tube, hMSC + MS tube and a section of rat trachea (after 1 freeze/thaw) compressed by a hand-held pipet to show repetitive luminal collapse and recoil of the tubes.

Supplementary video related to this article can be found at http://dx.doi.org/10.1016/j.biomaterials.2015.01.073.

2.10. Statistical analysis

One-way ANOVA with Tukey's post hoc tests were used to statistically analyze tissue engineered constructs and native tracheas via InStat 3.06 software (GraphPad Software Inc., La Jolla, CA). All values are reported as mean ± standard deviation. Post tests were performed when $p < 0.05$.

3. Results

3.1. Microsphere characterization

Gelatin microspheres appeared blue as a result of the crosslinking reaction with genipin. They were 26.6 ± 8.0% crosslinked, and their average diameter was 67.8 ± 55.1 μm (N = 268). A representative light microscopy image shows microspheres size variability (Fig. 2).

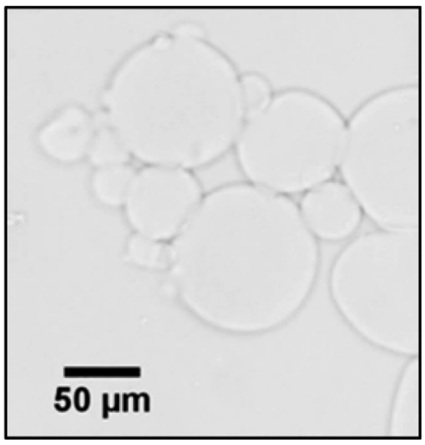

Fig. 2. Light photomicrograph of crosslinked gelatin microspheres.

3.2. Self-assembly of microsphere-containing tissue rings and manual assembly of tubes at day 2

Several hours after seeding, hMSC and hMSC + MS rings had self-assembled around the posts. After 2 days of culture, hMSC microsphere-containing rings appeared thicker and darker due to presence of microspheres compared to hMSC-only tissues, which were opaque off-white (Fig. 3A and C). The surface of hMSC + MS rings was less smooth compared to that of hMSC-only rings. Both hMSC-only and hMSC + MS rings could be handled with tweezers for tissue tube assembly into 3-ring or 6-ring tubes (Fig. 3B and D), but microsphere-containing rings held their toroid shape better during transfer from the agarose posts to the silicone tubes.

3.3. Gross morphological assessment

Tissues harvested after 22 days of total culture were firm and could be easily handled. The thickness of hMSC-only rings was more irregular compared to microsphere-containing rings, which were visually thicker and slightly blue due to residual microspheres that were not fully degraded (Fig. 4A and D). Stacked rings formed fused 3-ring or 6-ring tissue tubes on the 2 mm silicone tubing (Fig. 4B,C,E,F). Rings and 3-ring tissue tubes were pink due to residual media in the tissue, while 6-ring tissue tubes and rat tracheas were rinsed in PBS before being photographed. Similar to the microsphere-containing rings, tubes with microspheres were visually thicker than hMSC-only tubes. hMSC + MS tubes were also longer than the hMSC-only tubes. Incorporation of microspheres contributed to formation of ridged surfaces on tubes compared to smooth surfaces on hMSC-only tubes. Rat tracheas had visibly thinner walls compared to tissue engineered tubes (Fig. 4G).

3.4. Biochemical analysis

Individual rings and 3-ring tubes were analyzed biochemically. As expected, DNA (Fig. 5A), an indirect measure of cell number, and GAG (Fig. 5B) content were significantly greater in tubes compared

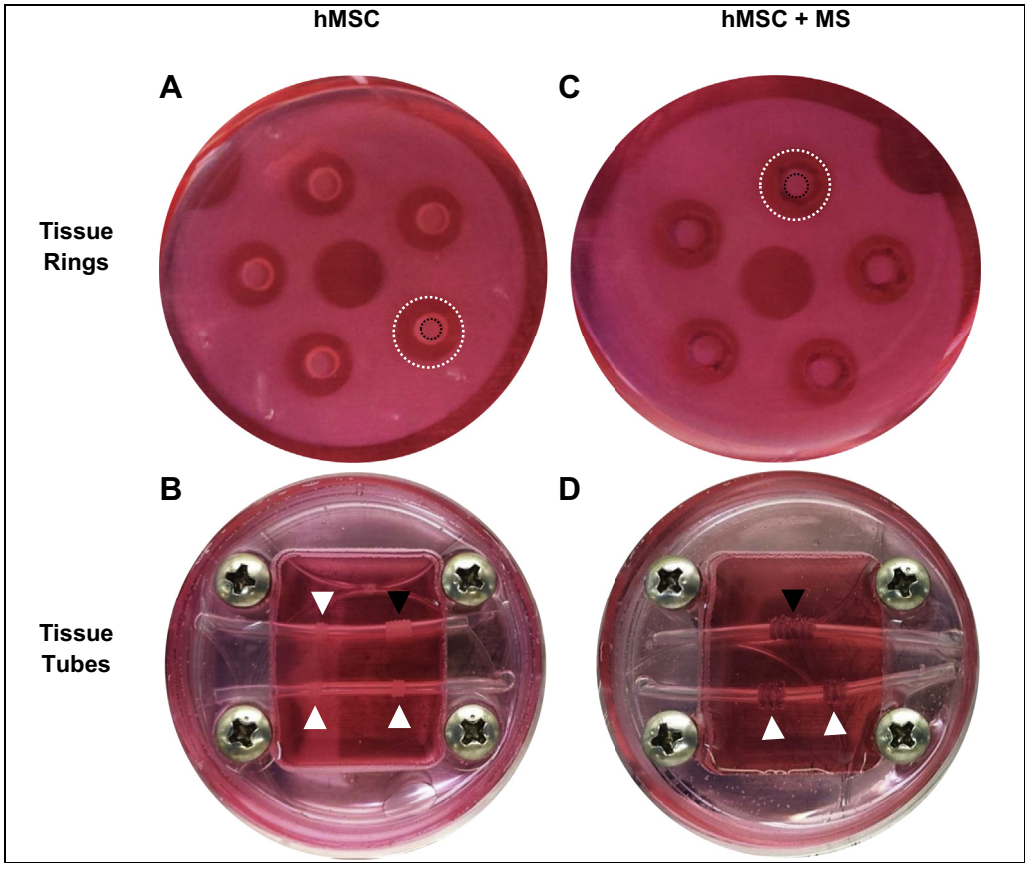

Fig. 3. Macroscopic images of tissue rings and tubes in culture. Tissue rings were formed by seeding a suspension of (A) hMSCs or (C) hMSCs with microspheres in custom designed agarose annular wells (white dotted outline) with 2 mm posts (black dotted outline). (B, D) On Day 2, some of the rings were stacked on silicone tubes, which were clamped in a custom designed holder, to form 3-ring (white arrow) or 6-ring (black arrow) tissue tubes. MS = Microspheres.

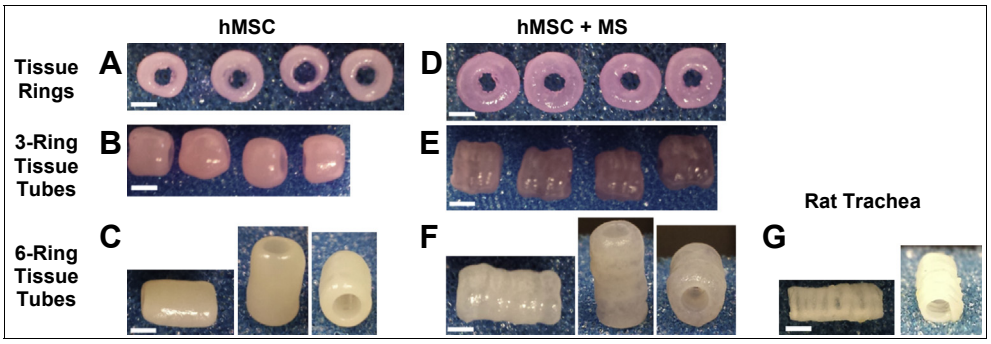

Fig. 4. Gross macroscopic pictures of (A–C) hMSC-only rings and tubes, (D–F) microsphere-containing rings and tubes, and (G) native rat trachea. (A, B, D, E) Rings and 3-ring tubes are shown in replicates. (C, F, G). A representative hMSC or hMSC + MS 6-ring tube and a rat trachea are presented from multiple perspectives. MS = Microspheres. Scale bar is 2 mm.

to individual rings because 3 rings were used for each tube. There was no significant increase in GAG production per DNA (Fig. 5C) in tissues grown in ring compared to tube geometries. Addition of growth factor-delivering microspheres did not significantly affect the cell number at the time of harvest as measured by amount of DNA. However, microspheres significantly increased total GAG and GAG production per cell. GAG/DNA was greater in hMSC + MS tissues than those without MS by factors of 2.2 and 1.7 in rings and tubes, respectively.

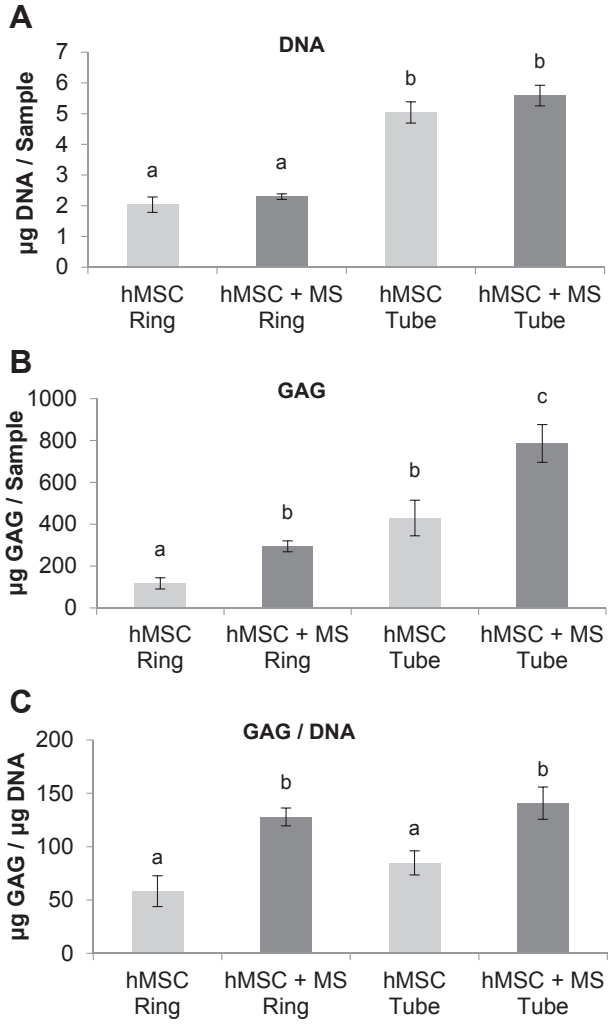

Fig. 5. (A) DNA content, (B) GAG content, and (C) GAG normalized to DNA in harvested rings and 3-ring tubes. MS = Microspheres. Groups that do not share the same letter are significantly different ($p < 0.01$).

3.5. Histology and immunohistochemistry

Safranin O with a Fast Green counterstain was used to visualize the presence and distribution of GAG in tissue engineered rings (Fig. 6A and C), 3-ring tubes (Fig. 6B and D) and rat trachea (Fig. 6E). Rings and tubes with microspheres (Fig. 6C and D) stained more intensely for GAG compared to cell-only constructs (Fig. 6A and B), corroborating the biochemical analysis. hMSC + MS rings and tubes were also visually thicker and had a more uniform GAG distribution with a smaller fibrous capsule (stained blue/green by Fast Green) on the tissue periphery compared to the hMSC-only tissues. The remaining gelatin microspheres that were not fully degraded by cell-secreted enzymes were visible in the hMSC + MS groups (black arrows in Fig. 6C and D). Cartilaginous portions of the rat trachea had the most intense GAG staining. Vertical cross sections of tissue engineered tubes of both compositions showed seamless ring fusion. hMSC-only tubes appeared to have lower GAG density in the middle of the constructs. Microsphere-containing tubes maintained ridges from the individual rings that were fused together. Cartilage rings in the rat trachea were separated by non-cartilaginous fibrous tissue, which stained blue/green.

The presence and distribution of collagen type II were visualized via immunohistochemical staining (Fig. 7). hMSC and hMSC + MS rings and tubes both showed strong staining for type II collagen, which was more prevalent on the interior of the constructs. However, staining was better distributed in microsphere-containing tissues. Human knee tissue control showed appropriate collagen type II staining of articular cartilage and no staining of the subchondral bone.

3.6. Tissue dimension measurements and biomechanical analysis

3.6.1. Rings

The walls of engineered hMSC-only and hMSC + MS cartilaginous rings were significantly thicker than those of native rat tracheas (Fig. 8A). Incorporation of microspheres resulted in rings that were significantly thicker than their cell-only counterparts. Uniaxial tension mechanical testing (Fig. 9A inset) revealed that the maximum force at failure (Fig. 9A) was similar in the engineered rings, but rat tracheal rings required a significantly smaller load to rupture. However, when force at failure was normalized to loaded area (ultimate tensile stress; Fig. 9B), microsphere-containing rings

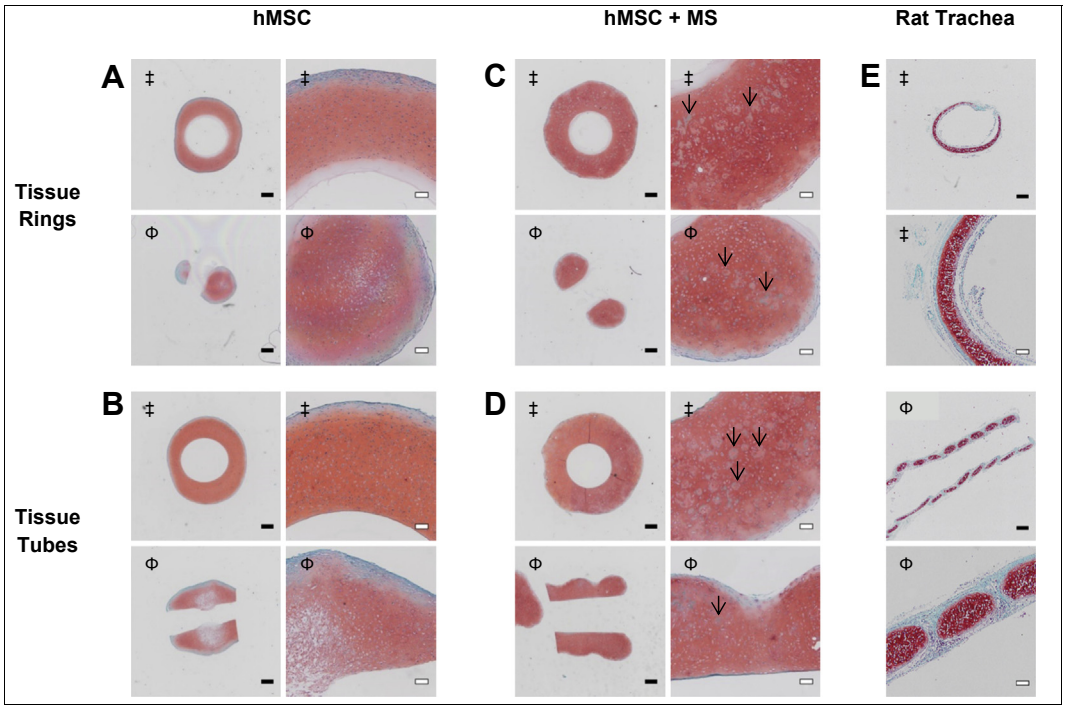

Fig. 6. Photomicrographs of Safranin O/Fast Green stained tissue engineered (A, C) rings and (B, D) tubes composed of (A, B) hMSCs-only and (C, D) hMSCs + MS, and (E) rat trachea in axial and vertical planes. Glycosaminoglycan-rich tissues are red/orange. Remnant gelatin microspheres (black arrows) are visible in hMSC + MS tissues. MS = Microspheres; Φ = axial plane; ‡ = vertical plane; black scale bars = 500 μm; white scale bars = 100 μm. (For interpretation of the references to color in this figure legend, the reader is referred to the web version of this article.)

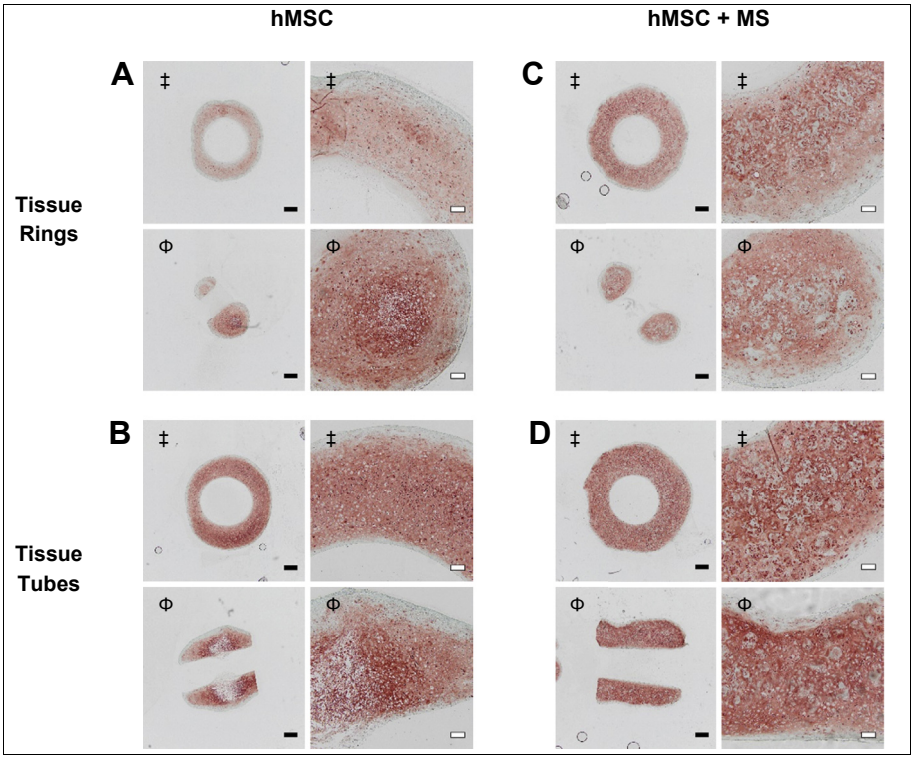

Fig. 7. Photomicrographs of Collagen Type II/Fast Green stained tissue engineered (A, C) rings and (B, D) tubes composed of (A, B) hMSCs-only (A, B) and (C, D) hMSCs + MS in axial and vertical planes. Type II collagen − rich tissues are red. MS = Microspheres; Φ = axial plane; ‡ = vertical plane; black scale bars = 500 μm; white scale bars = 100 μm. (For interpretation of the references to color in this figure legend, the reader is referred to the web version of this article.)

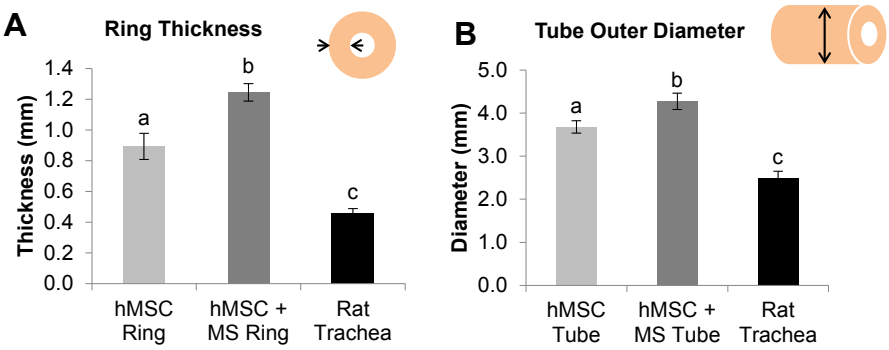

Fig. 8. (A) Ring thicknesses and (B) tube outer diameters measured in tissue engineered rings and tubes, and rat tracheas. MS = Microspheres. Groups that do not share a letter are significantly different ($p < 0.05$).

(2.44 ± 0.22 mm^2 cross-sectional area) behaved similarly to the rat trachea (1.22 ± 0.16 mm long; 1.11 ± 0.19 mm^2 cross-sectional area), while hMSC-only rings (1.26 ± 0.24 mm^2 cross-sectional area) exhibited significantly greater stress at failure than the other two groups.

3.6.2. Tubes

Tissue engineered tubes had a significantly greater outer diameter than the rat tracheas (Fig. 8B). In addition, microspheres containing tubes had a significantly greater outer diameter than hMSC tubes. In a gross biomechanical assessment of the tissue tubes, the qualitative force required to collapse the tubes with a hand-held pipet was the largest for the hMSC + MS tube (Video S1). Quantitative mechanical analysis corroborated the qualitative findings. A force was applied to collapse the tubes by 2 mm, the engineered tissues' inner diameter (Fig. 9C inset). The force required to collapse 80% of the lumen of engineered hMSC + MS tubes was ~2.1–2.3 times greater than the force required to collapse hMSC-only tubes and similarly-sized, 8 mm length sections of rat tracheas (Fig. 9C). Cell-only tubes required approximately the same load to achieve luminal collapse compared to the hMSC + MS tubes. After the load was removed, the outer diameters of the tubes were measured again and it was found that all tubes recoiled to nearly 100% of their original diameters (Fig. 9D).

4. Discussion

The trachea is a complex organ with multiple tissue types that provide specific function to the organ. A series of 18–22 incomplete and sometimes bifid cartilage rings provide mechanical integrity and prevent airway collapse [5,45]. Rings are completed by smooth muscle tissue called the trachealis which runs along the dorsal side of the trachea [5]. Each cartilage/smooth muscle ring is embedded in an elastic fibrous membrane which provides longitudinal flexibility and more importantly serves as a conduit for the vascular supply to the inside of the trachea [5,45]. The lumen is lined with a

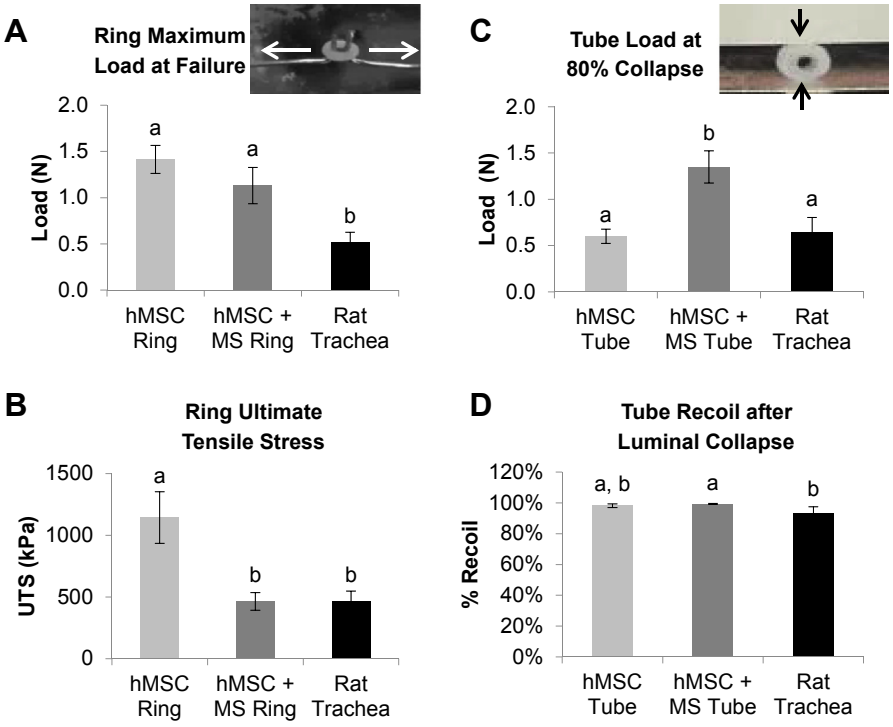

Fig. 9. Mechanical analysis of tissue engineered rings and tubes, and rat tracheas. (A) Ring maximum load at failure and (B) ultimate tensile stress during uniaxial testing (A, inset); (C) tube load at 80% collapse and (D) % recoil after luminal collapse (C, inset). MS = Microspheres. Groups that do not share the same letter are significantly different ($p < 0.05$).

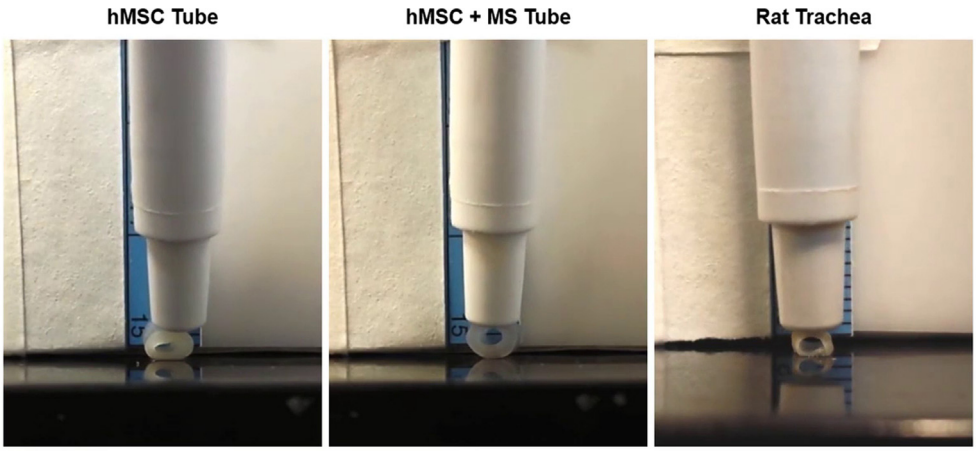

Video S1. A video still of repeated manual compression and release of a representative hMSC tube, hMSC + MS tube and a section of a rat trachea. MS = Microspheres. (The video recording can be viewed in the electronic version of this manuscript).

mucosal layer which contains a respiratory epithelium capable of interfacing with the external environment [5,45]. Considering the intricate and well-defined spatial distribution of tissues making up the tracheal anatomy, a modular tissue engineering strategy may prove valuable for airway regeneration. Specifically, ring shaped tissues can be used to build a tubular trachea replacement via a bottom-up approach using multiple cell-types in the radial and longitudinal directions. Additionally, bioactive microspheres can be incorporated into the constructs to enhance neotissue formation (e.g., amount and type of matrix production, matrix distribution, mechanical properties, etc.), provide spatial and temporal control over signal presentation, reduce time of *in vitro* culture, and support organogenesis after implantation.

The first goal of this study was to demonstrate the ability to form cartilaginous rings from human bone marrow-derived MSCs in custom culture wells and stack the rings to generate fused tissue tubes. Secondly, this work tested the hypothesis that incorporation of microspheres delivering chondrogenic growth factor (i.e., TGF-β1) into the self-assembled ring- and tube-shaped constructs would enhance neocartilage formation by increasing matrix production, tissue dimensions and mechanical properties. Custom annular culture wells comprised of agarose were used to successfully engineer hMSC-only and microsphere containing rings. On day 2 of culture, rings could be manipulated and stacked onto a silicone tube to fuse into tissue tubes. The two days of culture needed in this study is a much shorter time than the previously reported 3–4 week culture period necessary for high-cell density chondrocyte sheets to achieve mechanical integrity required for manual manipulation [25]. After approximately 3 weeks of culture, tubes were easily removed from the silicone support and exhibited seamless fusion between rings as observed via gross morphological and histological evaluation (Figs. 4, 6 and 7). The homogenous fusion between 2-day-old high-density hMSC-derived cartilage rings are consistent with the previously reported fusion of high-density hMSC pellets undergoing chondrogenesis [34]. The presence of GAG (Figs. 5 and 6) and collagen II (Fig. 7) indicated cartilaginous tissue formation after 22 days of total culture. These findings confirmed that custom agarose molds can be used to engineer cartilaginous rings and that these rings can be fused into tissue tubes.

While there are reports describing fabrication of rabbit auricular chondrocyte-derived cartilage sheets that were rolled to fuse into a tube *in vitro* [26,46] or *in vivo* [21], our approach has critical advantages over these systems. First of all, human bone marrow MSCs used here as the cell source for autologous cartilage tissue formation avoids the need for invasive and potentially detrimental harvest of mature cartilage tissues and provides the capacity for cell expansion to achieve necessary numbers of cells capable of undergoing chondrogenesis. In addition, the use of human cells in our system is potentially a more translatable strategy, as approaches utilizing cells from different species may result in different chondrogenic outcomes compared to those with human cells [30,47], delaying or inhibiting transfer of technology to the clinical setting. Secondly, the hMSC-based cartilaginous rings in this report were significantly thicker than previously reported chondrocyte-based approaches. In just 3 weeks of culture, hMSC-derived cartilage rings were 0.89 mm (hMSC-only) and 1.25 mm (hMSC + MS) thick compared to rabbit articular chondrocyte-derived cartilage, which was 235 μm thick after 8 weeks of culture [25], and rabbit auricular chondrocyte-derived cartilage, which was ~500 μm thick after 6 weeks of culture [26] and 553 μm thick after 8 weeks of culture [25]. To achieve wall thicknesses similar to those found in our hMSC-based rings, multiple cartilage sheets would need to be stacked or folded [21,46]. Thirdly, in terms of cartilage tube fabrication, the ring assembly system does not require the binding of tissue sheets with sutures or ties to form a tubular construct [21,26]. More importantly, our ring-based approach is a modular system which could prove advantageous when generating multi-tissue type constructs because each ring could serve as a tissue building block. Finally, the ring-to-tube technology may be more favorable in resisting compression in the axial plane, thereby maintaining tracheal patency in future *in vivo* applications, compared to sheet-to-tube technologies which may have heterogeneous mechanical properties around the circumference of the tube. While rat hepatocyte cell line rings [48] and 2-ring tubes [49], normal human fibroblast rings [48] and smooth muscle cell rings and tubes [35] have been reported, the fabrication of scaffold-free, stem cell-based cartilage-like rings and tubes using a custom ring and tube assembly system has not yet been demonstrated.

To address the second goal of this work, the degree of chondrogenesis was compared between tissues developed from high-density hMSC ring and tube cultures containing proteolytically-degradable TGF-β1-loaded gelatin microspheres and hMSC-only tissues grown in the same geometries with exogenously delivered growth factor. This high-cell density culture system with bioactive microspheres has previously been shown to enhance chondrogenesis, mechanical properties and/or tissue thickness in hMSC-derived aggregate and sheet constructs [36,38,39]. In the present work, tissues with bioactive microspheres were visually thicker

(both rings and tubes) and longer (tubes) than hMSC-only constructs. Tubes created from microsphere containing rings maintained outer ridge morphology reminiscent of the rings used for fusion (Figs. 4E, F and 6D). It is possible that even after only 2 days of culture, incorporation of TGF-β1-loaded microspheres encouraged greater and/or more mature matrix deposition in tissue rings, making the remodeling of ECM more challenging during the fusion process. Another possible reason for the presence of ridges in the hMSC + MS tubes is that incorporation of microspheres led to a more uniform cartilaginous matrix distribution and a reduced fibrous capsule, which has been reported to encourage cartilage tissue fusion [50]. This GAG-poor capsule, sometimes seen on the periphery of high-cell density cultures [39], was more prevalent in hMSC-only tissues and may be the reason for smoother surfaces found in hMSC-only tubes (Fig. 6A and B) compared to the GAG-rich, ribbed hMSC + MS tubes (Fig. 6C and D).

Incorporation of growth factor-loaded microspheres enhanced chondrogenesis as detected by biochemical and histological assays and measurement of tissue dimensions. This finding is corroborated by previous reports of improved cartilage formation in high-density hMSC systems with incorporated TGF-β1-loaded gelatin microspheres [38,39]. Compared to hMSC-only rings and tubes, hMSC + MS rings and tubes produced more GAG per DNA (Fig. 5C) and stained more intensely for GAG (Fig. 6) and collagen type II (Fig. 7), which are all indicative of neocartilage formation [47]. Not only was the ECM more cartilaginous, addition of growth factor loaded microspheres led to increased tissue ring thickness and tube outer diameter (Fig. 8). Taken all together, the biochemical, histological and tissue dimension data supported our hypothesis that incorporation of growth-factor-loaded microspheres into the hMSC high-cell density rings and tubes improved chondrogenesis in the constructs.

Upon mechanical evaluation of tissue engineered rings and tubes, incorporation of microspheres decreased ring tensile strength and did not affect tubular luminal elasticity. Uniaxial UTS values showed that incorporation of microspheres resulted in a lower stress at failure (Fig. 9B). Even though the load at failure was only slightly lower in hMSC + MS rings than hMSC-only rings (no significant difference; Fig. 9A), the hMSC + MS rings had a significantly greater cross-sectional area (Fig. 8A) resulting in a significantly smaller UTS. Still, reduced UTS values were an unexpected finding since incorporation of growth factor-laden microspheres has been shown to increase the equilibrium compressive moduli of hMSC-derived engineered cartilage sheets [39]. However, in the present study, the residual gelatin microspheres that were not fully degraded could have been acting as inclusions, thereby weakening the tissues' tensile strength. Another potential explanation for decreased UTS is the differences in biochemical make-up of the ECM in the hMSC + MS compared to hMSC-only rings. The GAG content is a dominant contributor to increased tissue stiffness in compression [51] and collagen content is predominantly responsible for tensile properties [52] in cartilage tissues. While the addition of microspheres significantly increased GAG biochemical content as well as GAG and type II collagen staining, it is possible that microspheres led to a greater relative increase in GAG compared to collagen resulting in lower tensile properties in the hMSC + MS rings than the hMSC-only rings. Mechanical evaluation of tissue tubes showed that all tissue tubes recoiled to almost the original outer diameter, but microsphere-containing tissues required greater force to collapse the tubes. However, microsphere containing tubes were also qualitatively longer than their cell-only counterparts so it is difficult to examine the role that microspheres played on the luminal elasticity mechanics of the tissue tubes.

Tissue generation was influenced by culture in the custom wells and assembly system in the ring and tube geometries. Three-ring tubes had significantly greater DNA and GAG content than individual rings, although these increases were slightly less than the 3-fold proportional increases that would be expected. However, GAG production per cell was not significantly different between ring and tube geometries. Unexpectedly, both geometeries (with and without microspheres) led to approximately two-fold greater GAG/DNA production compared to high-cell density sheets grown on cell culture inserts using same passage hMSCs from the same donor as used in this study (Supplementary Fig. 1). It is possible that the agarose culture wells limited the diffusion of ECM molecules produced by cells into the bulk medium, thereby increasing their effective concentration in the constructs and the probability of macromolecule assembly and matrix maturation. For example, aggrecan, a cartilage-specific proteoglycan which plays an important role in resisting cartilage compression during loading, is non-covalently bound to hyaluronic acid and stabilized by link protein to form large aggrecan aggregates outside the cell [53]. Collagen fiber bundles are also assembled extracellularly. Additionally, proteoglycan–collagen interaction is essential for cartilaginous ECM function [54]. A potentially similar biophysical approach called macromolecular crowding, which incorporates large molecules as a means of increasing medium density and limiting diffusion, has been shown to drastically increase deposition of type I collagen by fibroblasts in tissue culture [55]. Another possibility for improved chondrogenesis is the increased surface area to volume ratio of the toroid compared to sheet culture for the same number of cells, which could result in greater availability of oxygen and nutrients and better removal of waste via diffusion.

The custom well and assembly system presented in this work was used to engineer a tracheal replacement which can be initially tested in a small animal model for tracheal defects – the rat. With regard to tissue dimensions, rat tracheas have a similar lumen diameter but the walls of engineered rings were significantly thicker (Fig. 8A) and tubes had significantly greater outer diameters (Fig. 8B) compared to rat tracheas. Mechanical evaluation by uniaxial UTS on the rings and luminal collapse and recoil on the tubes showed that scaffold-free cartilaginous rings and tubes perform at least as well as native rat trachea, suggesting that these engineered tissues may be able to provide the mechanical rigidity necessary to maintain airway patency in the rat. It is promising that the tissue engineered microsphere-containing neocartilaginous tubes required significantly greater loads to collapse the lumen compared to the similarly-sized rat tracheal segments because a trachea for clinical use in humans will likely need to be stiffer than a rat trachea. While tissue engineered cartilage rings and tubes appeared thicker than rat tracheal cartilage, they are very similar to the thickness of human tracheal cartilage rings. Unlike the tissue engineered torus rings with a circular cross-section presented here, human tracheal cartilage rings are toroid-like with a more rectangular-shaped cross-sectional area which is typically ~1 mm radially and ~4 mm vertically [45]. Control over the vertical dimension of engineered tubes can be achieved by fusing multiple rings together, as shown in this study. A longer engineered trachea would simply require more cells, microspheres, growth factor and media, but tissue generation should not be inhibited by the length of the construct. Adult human trachea also has a much larger lumen, measuring at least 12 mm in diameter [45], but using this approach it will be possible to engineer larger diameter rings and tubes by modifying the size of the cell culture annular wells for ring self-assembly and the support strut for tube culture. Additionally, the geometry of the culture wells and the tissue assembly approach can be easily altered to produce self-assembled tissues of specific shapes (e.g., oval tissues with defined wall thickness, cone like structures, or even figure-eight, honeycomb and dog bone shaped

constructs [56]) for applications necessitating geometrical control over anatomical features and/or tissue-level morphology.

A functional tracheal replacement may require much more complexity in tissue organization and function. For this reason, the work presented here is an important step for engineering necessary building blocks for a viable tracheal replacement therapy. While the cartilaginous portion of the native trachea provides support to the airway, intervening vascularized fibrous tissue is necessary to supply the cartilaginous rings and mucosal and submucosal layers lining the tracheal lumen with nutrients and oxygen. Our customizable tissue assembly system may permit the integration of these vital tissue components to replicate actual tracheal architecture and ultimately function. Firstly, donor-specific needs with regard to tissue anatomy may be addressed by employing annular wells and support struts with custom geometry to engineer the organ [5]. Next, different cell sources and/or differentiation conditions for the tissue units can be used to engineer tissues with requisite properties, such as rings with neovasculogenic capabilities or tubes of tracheal epithelium. Thirdly, incorporation of bioactive microspheres with different compositions into each type of tissue ring may allow for spatial as well as temporal control of cell differentiation and neotissue formation even after multi-tissue fusion. It is also possible that incorporation of growth factor-loaded microspheres can decrease *in vitro* culture time by releasing bioactive factors after implantation, and in doing so stimulate *in vivo* tissue maturation and physiological healing. Although further research is necessary to determine multi-tissue culture conditions, the use of bioactive microspheres in the modular custom culture system described here is a promising approach for tracheal tissue regeneration.

5. Conclusion

A customizable, modular technology was used to develop cartilaginous tissue structures that have the potential to serve as viable building blocks for tracheal tissue engineering. This work demonstrates the use of a modular system to engineer cartilaginous scaffold-free, high-cell density rings and their subsequent successful fusion into cartilage tubes. In addition, a bioactive factor delivery system was employed to enhance neocartilage formation with regard to cartilaginous matrix production, tissue dimensions and some mechanical properties of self-assembled hMSC rings and tubes. Engineered rings and tubes had similar, if not improved, biomechanical properties compared to native rat trachea, suggesting that airway patency could be maintained in a tracheal replacement in this animal model. Importantly, the customizable, modular culture system with bioactive factor delivery can be tailored to not only engineer tissues of variable geometries and sizes, but also mixed cell and tissue types in order to recapitulate the elaborate organization necessary for generating a human neotrachea.

Acknowledgments

The authors thank Amad Awadallah for providing excellent histological services and Zijie Zheng for conducting the ninhydrin assay. This work was supported by the National Institutes of Health (R01AR063194 (EA) and T32AR007505 (ADD)), the Medtronic Foundation (ADD) and NSF IGERT DGE 1144804 (MWR and HAS).

Appendix A. Supplementary data

Supplementary data related to this article can be found at http://dx.doi.org/10.1016/j.biomaterials.2015.01.073.

References

[1] ten Hallers EJ, Rakhorst G, Marres HA, Jansen JA, van Kooten TG, Schutte HK, et al. Animal models for tracheal research. Biomaterials 2004;25(9):1533–43.
[2] Gomez-Caro A, Morcillo A, Wins R, Molins L, Galan G, Tarrazona V. Surgical management of benign tracheal stenosis. Multimed Man Cardiothorac Surg 2011;2011(1111). mmcts 2010 004945.
[3] Welkoborsky HJ, Hinni ML, Moebius H, Bauer L, Ostertag H. Microscopic examination of iatrogenic subglottic tracheal stenosis: observations that may elucidate its histopathologic origin. Ann Otol Rhinol Laryngol 2014;123(1):25–31.
[4] Grillo HC. Tracheal replacement: a critical review. Ann Thorac Surg 2002;73(6):1995–2004.
[5] Grillo HC. Surgery of the trachea and bronchi. Hamilton, Ontario: BC Decker Inc; 2004.
[6] Nesek-Adam V, Mrsic V, Oberhofer D, Grizelj-Stojcic E, Kosuta D, Rasic Z. Post-intubation long-segment tracheal stenosis of the posterior wall: a case report and review of the literature. J Anesth 2010;24(4):621–5.
[7] Okumura N, Nakamura T, Natsume T, Tomihata K, Ikada Y, Shimizu Y. Experimental study on a new tracheal prosthesis made from collagen-conjugated mesh. J Thorac Cardiovasc Surg 1994;108(2):337–45.
[8] Omori K, Nakamura T, Kanemaru S, Asato R, Yamashita M, Tanaka S, et al. Regenerative medicine of the trachea: the first human case. Ann Otol Rhinol Laryngol 2005;114(6):429–33.
[9] Tatekawa Y, Kawazoe N, Chen GP, Shirasaki Y, Komuro H, Kaneko M. Tracheal defect repair using a PLGA-collagen hybrid scaffold reinforced by a copolymer stent with bFGF-impregnated gelatin hydrogel. Pediatr Surg Int 2010;26(6):575–80.
[10] Fabre D, Kolb F, Fadel E, Mercier O, Mussot S, Le Chevalier T, et al. Successful tracheal replacement in humans using autologous tissues: an 8-year experience. Ann Thorac Surg 2013;96(4):1146–55.
[11] Ch'ng S, Wong GL, Clark JR. Reconstruction of the trachea. J Reconstr Microsurg 2014;30(3):153–62.
[12] Delaere P, Liu Z, Feenstra L. Experimental tracheal revascularization and transplantation. Acta Otorhinolaryngol Belg 1995;49(4):407–13.
[13] Delaere P, Vranckx J, Verleden G, De Leyn P, Van Raemdonck D, Leuven Tracheal Transplant G. Tracheal allotransplantation after withdrawal of immunosuppressive therapy. N Engl J Med 2010;362(2):138–45.
[14] Jungebluth P, Bader A, Baiguera S, Moller S, Jaus M, Lim ML, et al. The concept of in vivo airway tissue engineering. Biomaterials 2012;33(17):4319–26.
[15] Macchiarini P, Jungebluth P, Go T, Asnaghi MA, Rees LE, Cogan TA, et al. Clinical transplantation of a tissue-engineered airway. Lancet 2008;372(9655):2023–30.
[16] Elliott MJ, De Coppi P, Speggiorin S, Roebuck D, Butler CR, Samuel E, et al. Stem-cell-based, tissue engineered tracheal replacement in a child: a 2-year follow-up study. Lancet 2012;380(9846):994–1000.
[17] Haykal S, Salna M, Zhou Y, Marcus P, Fatehi M, Frost G, et al. Double-chamber rotating bioreactor for dynamic perfusion cell seeding of large-segment tracheal allografts: comparison to conventional static methods. Tissue Eng Part C Methods 2014;20(8):681–92.
[18] Berg M, Ejnell H, Kovacs A, Nayakawde N, Patil PB, Joshi M, et al. Replacement of a tracheal stenosis with a tissue-engineered human trachea using autologous stem cells: a case report. Tissue Eng Part A 2014;20(1–2):389–97.
[19] Vacanti CA, Paige KT, Kim WS, Sakata J, Upton J, Vacanti JP. Experimental tracheal replacement using tissue-engineered cartilage. J Pediatr Surg 1994;29(2):201–4. discussion 4–5.
[20] Kunisaki SM, Freedman DA, Fauza DO. Fetal tracheal reconstruction with cartilaginous grafts engineered from mesenchymal amniocytes. J Pediatr Surg 2006;41(4):675–82. discussion-82.
[21] Weidenbecher M, Tucker HM, Awadallah A, Dennis JE. Fabrication of a neotrachea using engineered cartilage. Laryngoscope 2008;118(4):593–8.
[22] Komura M, Komura H, Otani Y, Kanamori Y, Iwanaka T, Hoshi K, et al. The junction between hyaline cartilage and engineered cartilage in rabbits. Laryngoscope 2013;123(6):1547–51.
[23] Tan Q, Steiner R, Hoerstrup SP, Weder W. Tissue-engineered trachea: history, problems and the future. Eur J Cardiothorac Surg 2006;30(5):782–6.
[24] Athanasiou KA, Eswaramoorthy R, Hadidi P, Hu JC. Self-organization and the self-assembling process in tissue engineering. Annu Rev Biomed Eng 2013;15:115–36.
[25] Whitney GA, Mera H, Weidenbecher M, Awadallah A, Mansour JM, Dennis JE. Methods for producing scaffold-free engineered cartilage sheets from auricular and articular chondrocyte cell sources and attachment to porous tantalum. BioResearch Open Access 2012;1(4):157–65.
[26] Tani G, Usui N, Kamiyama M, Oue T, Fukuzawa M. In vitro construction of scaffold-free cylindrical cartilage using cell sheet-based tissue engineering. Pediatr Surg Int 2010;26(2):179–85.
[27] Hubka KM, Dahlin RL, Meretoja VV, Kasper FK, Mikos AG. Enhancing chondrogenic phenotype for cartilage tissue engineering: monoculture and coculture of articular chondrocytes and mesenchymal stem cells. Tissue Eng Part B Rev 2014;20(6):641–54.
[28] Caplan AI. Mesenchymal stem cells. J Orthop Res 1991;9(5):641–50.
[29] Pittenger MF, Mackay AM, Beck SC, Jaiswal RK, Douglas R, Mosca JD, et al. Multilineage potential of adult human mesenchymal stem cells. Science 1999;284(5411):143–7.

[30] Johnstone B, Hering TM, Caplan AI, Goldberg VM, Yoo JU. In vitro chondrogenesis of bone marrow-derived mesenchymal progenitor cells. Exp Cell Res 1998;238(1):265–72.
[31] Mackay AM, Beck SC, Murphy JM, Barry FP, Chichester CO, Pittenger MF. Chondrogenic differentiation of cultured human mesenchymal stem cells from marrow. Tissue Eng 1998;4(4):415–28.
[32] Murdoch AD, Grady LM, Ablett MP, Katopodi T, Meadows RS, Hardingham TE. Chondrogenic differentiation of human bone marrow stem cells in transwell cultures: generation of scaffold-free cartilage. Stem Cells 2007;25(11):2786–96.
[33] Huey DJ, Athanasiou KA. Maturational growth of self-assembled, functional menisci as a result of TGF-beta1 and enzymatic chondroitinase-ABC stimulation. Biomaterials 2011;32(8):2052–8.
[34] Bhumiratana S, Eton RE, Oungoulian SR, Wan LQ, Ateshian GA, Vunjak-Novakovic G. Large, stratified, and mechanically functional human cartilage grown in vitro by mesenchymal condensation. Proc Natl Acad Sci U S A 2014;111(19):6940–5.
[35] Gwyther TA, Hu JZ, Christakis AG, Skorinko JK, Shaw SM, Billiar KL, et al. Engineered vascular tissue fabricated from aggregated smooth muscle cells. Cells Tissues Organs 2011;194(1):13–24.
[36] Solorio LD, Fu AS, Hernandez-Irizarry R, Alsberg E. Chondrogenic differentiation of human mesenchymal stem cell aggregates via controlled release of TGF-beta1 from incorporated polymer microspheres. J Biomed Mater Res Part A 2010;92(3):1139–44.
[37] Dang PN, Solorio LD, Alsberg E. Driving cartilage formation in high-density human adipose-derived stem cell aggregate and sheet constructs without exogenous growth factor delivery. Tissue Eng Part A 2014;20(23-24):3163–75.
[38] Solorio LD, Dhami CD, Dang PN, Vieregge EL, Alsberg E. Spatiotemporal regulation of chondrogenic differentiation with controlled delivery of transforming growth factor-beta1 from gelatin microspheres in mesenchymal stem cell aggregates. Stem Cells Transl Med 2012;1(8):632–9.
[39] Solorio LD, Vieregge EL, Dhami CD, Dang PN, Alsberg E. Engineered cartilage via self-assembled hMSC sheets with incorporated biodegradable gelatin microspheres releasing transforming growth factor-beta1. J Control Release 2012;158(2):224–32.
[40] Haynesworth SE, Goshima J, Goldberg VM, Caplan AI. Characterization of cells with osteogenic potential from human marrow. Bone 1992;13(1):81–8.
[41] Lennon DP, Haynesworth SE, Bruder SP, Jaiswal N, Caplan AI. Human and animal mesenchymal progenitor cells from bone marrow: Identification of serum for optimal selection and proliferation. In Vitro Cell Dev An 1996;32(10):602–11.
[42] Ponticiello MS, Schinagl RM, Kadiyala S, Barry FP. Gelatin-based resorbable sponge as a carrier matrix for human mesenchymal stem cells in cartilage regeneration therapy. J Biomed Mater Res 2000;52(2):246–55.
[43] Farndale RW, Buttle DJ, Barrett AJ. Improved quantitation and discrimination of sulfated glycosaminoglycans by use of dimethylmethylene blue. Biochim Biophys Acta 1986;883(2):173–7.
[44] McGowan KB, Kurtis MS, Lottman LM, Watson D, Sah RL. Biochemical quantification of DNA in human articular and septal cartilage using PicoGreen and Hoechst 33258. Osteoarthr Cartilage 2002;10(7):580–7.
[45] Standring S, Borley NR, Collins P, Crossman AR, Gatzoulis MA, Healy JC, et al. Gray's anatomy: the anatomical basis of clinical practice. Elsevier; 2009.
[46] Gilpin DA, Weidenbecher MS, Dennis JE. Scaffold-free tissue-engineered cartilage implants for laryngotracheal reconstruction. Laryngoscope 2010;120(3):612–7.
[47] Yoo JU, Barthel TS, Nishimura K, Solchaga L, Caplan AI, Goldberg VM, et al. The chondrogenic potential of human bone-marrow-derived mesenchymal progenitor cells. J Bone Jt Surg Am 1998;80(12):1745–57.
[48] Dean DM, Napolitano AP, Youssef J, Morgan JR. Rods, tori, and honeycombs: the directed self-assembly of microtissues with prescribed microscale geometries. FASEB J 2007;21(14):4005–12.
[49] Livoti CM, Morgan JR. Self-assembly and tissue fusion of toroid-shaped minimal building units. Tissue Eng Part A 2010;16(6):2051–61.
[50] Yang YH, Ard MB, Halper JT, Barabino GA. Type I collagen-based fibrous capsule enhances integration of tissue-engineered cartilage with native articular cartilage. Ann Biomed Eng 2014;42(4):716–26.
[51] Buschmann MD, Grodzinsky AJ. A molecular model of proteoglycan-associated electrostatic forces in cartilage mechanics. J Biomech Eng 1995;117(2):179–92.
[52] Mow V, Ratcliffe A. Structure and function of articular cartilage and meniscus. 2nd ed. Philadelphia: Lippincott-Raven; 1997.
[53] Knudson CB, Knudson W. Cartilage proteoglycans. Semin Cell Dev Biol 2001;12(2):69–78.
[54] Junqueira LC, Montes GS. Biology of collagen-proteoglycan interaction. Arch Histol Jpn Nihon Soshikigaku Kiroku 1983;46(5):589–629.
[55] Satyam A, Kumar P, Fan X, Gorelov A, Rochev Y, Joshi L, et al. Macromolecular crowding meets tissue engineering by self-assembly: a paradigm shift in regenerative medicine. Adv Mater 2014;26(19):3024–34.
[56] Svoronos AA, Tejavibulya N, Schell JY, Shenoy VB, Morgan JR. Micro-mold design controls the 3D morphological evolution of self-assembling multicellular microtissues. Tissue Eng Part A 2014;20(7–8):1134–44.